

# HOMOGENEOUS METAL PARTS BY INFILTRATION

Adam M. Lorenz<sup>1</sup>, Emanuel M. Sachs<sup>1</sup>, Samuel M. Allen<sup>2</sup>, and Michael J. Cima<sup>2</sup>

<sup>1</sup>Department of Mechanical Engineering

<sup>2</sup>Department of Materials Science and Engineering

Massachusetts Institute of Technology, Cambridge, MA 02139

## Abstract

Infiltration of powdered metal parts made by SFF processes enables densification with negligible dimensional change, but typically uses a dissimilar infiltrant material resulting in poor corrosion resistance, machinability, and a heterogeneous composition inconducive to certification for critical applications. A new approach called transient liquid-phase infiltration is described using an infiltrant composition similar to that of the powder skeleton, but containing a melting point depressant. Upon infiltration, the liquid undergoes diffusional solidification at infiltration temperature and eventually the composition becomes homogeneous. Parts over 20 cm tall have been fabricated through careful selection of skeleton and infiltrant compositions, skeleton powder size, and infiltration technique. The work presented in this paper uses a nickel-silicon alloy to infiltrate a skeleton of pure nickel powder.

## Introduction

Several Solid Freeform Fabrication technologies use powdered metal as the raw material to produce a net shape part skeleton that is less than 70% dense. The skeleton must then undergo further processing to achieve full density and the desired mechanical properties. The densification is typically done either by light sintering and infiltration with a lower melting temperature alloy or by high temperature sintering alone. In the first method of densification, the part's dimensional change is typically only ~1%, making it suitable for fairly large (~0.5 m on a side) parts. However, the resulting material composition is a heterogeneous mixture of the powder material and the lower melting temperature infiltrant, often with poor machinability and corrosion resistance. In critical applications such as structural, aerospace and military, a material of homogeneous composition is preferable for certification. Sintering the powder to full density will result in a homogeneous final material, but a part will undergo ~15% linear shrinkage if it starts out at 60% density. For this reason, full density sintering is typically only used for smaller (< 5 cm on a side) parts.

This paper describes a process for making large, homogeneous parts from a powder skeleton using an infiltrant material similar in composition to the skeleton material, with the addition of a small amount of melting point depressant. The liquid infiltrant fills the void space in the skeleton, then undergoes diffusional solidification to achieve a homogeneous final part composition. The process is shown schematically in Figure 1 and is referred to here as Transient Liquid-phase Infiltration (TLI) due to the phase transition of the infiltrant. In some cases the diffusional solidification can prevent the infiltrant from filling a part skeleton. Determination of conditions that allow complete infiltration is a major focus of this work.

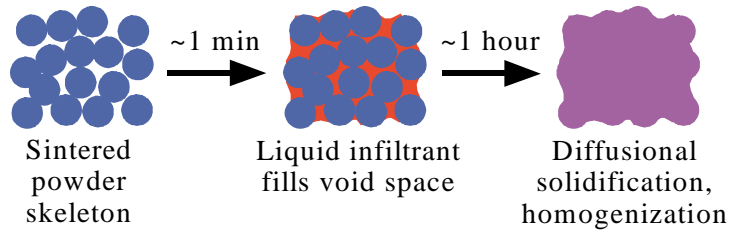


Figure 1: Transient Liquid-phase Infiltration

A nickel-based material system was chosen for development of the TLI concept because transient liquid-phase nickel brazing alloys are commonly used in the aerospace industry and nickel alloys are of interest in some DoD applications. Silicon was chosen as the melting point depressant primarily because it has a lower diffusivity than boron and phosphorous, the other common melting point depressant in nickel brazing alloys. In addition, silicon has a high enough solubility in nickel to allow complete solidification at the infiltration temperature. Figure 2 shows the nickel-rich side of the binary Ni–Si phase diagram<sup>1</sup> and points out the composition of the skeleton and infiltrant as well as the resulting homogenized composition at an infiltration temperature of 1180°C. The diffusivity of the melting point depressant affects the amount of time the liquid has to fill the skeleton before it freezes. The diffusivity of Si in Ni is  $\sim 10^{-13}$  m<sup>2</sup>/s at 1200°C, resulting in a characteristic diffusion distance of  $\sqrt{4D \cdot t} = 5$  μm after 1 minute. This is a sufficiently small distance to allow infiltration of nickel powders greater than 50 microns in diameter.

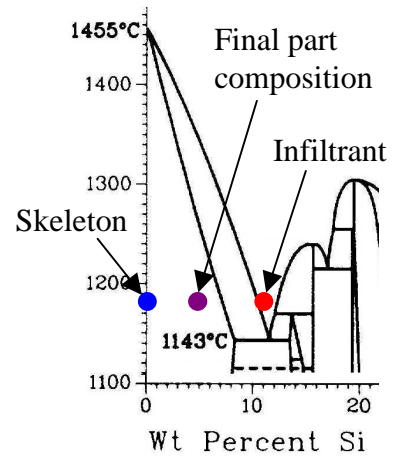


Figure 2: Ni–Si phase diagram.

### Study of Fluid Flow and Infiltration Rate

Infiltration is the result of capillary induced pressure driving the fluid into the skeleton. In a non-reactive system, fluid will continue to flow into the skeleton until the gravitational head,  $\rho gh$ , balances the capillary force. The maximum capillary rise height can be calculated accordingly:

$$h_{\max} = \frac{1}{\rho g} \left( \frac{\gamma_{LV} \cdot \cos(\theta) S_p}{V_p} \right) = \frac{6\gamma(1-\varepsilon)}{D\varepsilon\rho g} \quad (1)$$

where  $h$  is fluid height,  $\rho$  is the fluid density,  $g$  is gravity,  $\gamma_{LV}$  is the liquid/vapor interfacial energy,  $\theta$  is the contact angle of the liquid to the solid,  $S_p$  is the surface area of the pore space and  $V_p$  is the volume of the pore space.<sup>2</sup> The right most term in the equality lumps the wetting angle into the surface energy term  $\gamma = \gamma_{LV} \cdot \cos(\theta)$ , and assumes the powder bed is composed of uniform spheres of diameter  $D$  with a void fraction  $\varepsilon$  to substitute for the ratio of surface area to volume. Due to the high surface energy of most liquid metals, a skeleton of 100 μm powder will typically result in capillary rise heights greater than 1 meter. In TLI, this equilibrium condition may not be reached before the infiltrant freezes.

Because the liquid has a limited amount of time available to fill the skeleton, it is necessary to study the fluid flow behavior. Darcy's Law describes the flow of viscous fluid through porous media, stating that the pressure gradient will be directly proportional to the volume-averaged velocity of the fluid:

$$\nabla P = -\frac{\mu}{K}V$$

where  $\mu$  is the fluid viscosity and  $K$  describes the permeability of the porous body. The permeability of various powder skeletons was determined by measuring the flow rate of oil (Multitherm 503) through the skeletons at room temperature under known pressure conditions as shown in Figure 3 at right.<sup>3</sup> Skeletons for these and all subsequent experiments were composed of hydrometallurgically processed nickel powder sintered at 1200°C for 1 hour. Skeletons of 90–125  $\mu\text{m}$  and 212–300  $\mu\text{m}$  powder resulted in permeabilities of  $5.0 \times 10^{-12} \text{ m}^2$  and  $1.7 \times 10^{-11} \text{ m}^2$  respectively.

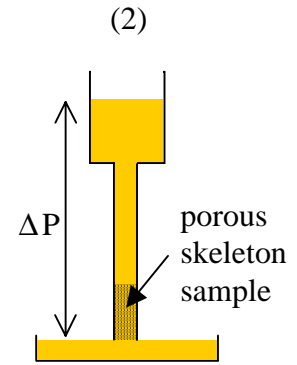


Figure 3: Permeametry.

The rate of infiltration into the skeleton was measured experimentally and compared to a model of the fluid flow based on Darcy's Law. The model uses the same assumptions as Equation 1 for the capillary driving force with an extra term for the head losses due to gravity:

$$\frac{dh}{dt} = \frac{K}{\epsilon\mu} \left( \frac{6\gamma(1-\epsilon)}{D\epsilon h} - \rho g \right) \quad (3)$$

Experiments were conducted at room temperature with oil and the results are shown in Figure 4. The measured permeability predicted a slightly faster infiltration than that observed experimentally, so a second curve is shown with permeability selected to match the experimental data. This permeability was 40% less than that measured by permeametry.

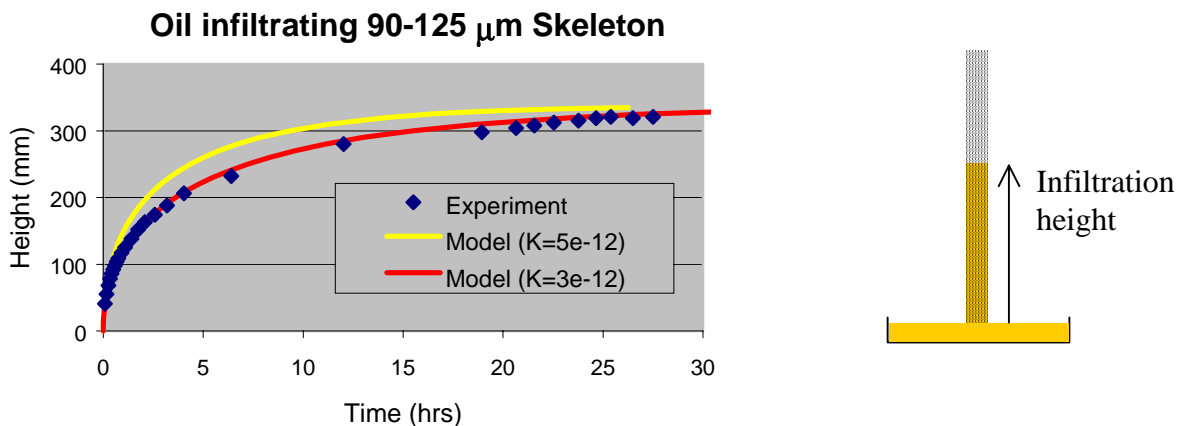


Figure 4: Infiltration rate experiments with oil at room temperature.

Measurements of the infiltration height of liquid metal inside the furnace was not directly observable, so the rate of infiltration was calculated based on mass increase. Figure 5 schematically shows the apparatus used to measure the mass of the skeleton during a transient liquid phase infiltration of a similar skeleton, along with experimental results. The skeleton was suspended from a 0.010" diameter molybdenum wire and the force on the wire was measured via

a load cell and a datalogger at 0.05 second intervals. The contribution due to surface tension was subtracted from the measured force, and the resulting value was converted to infiltration height by dividing by the density of the liquid and the cross-sectional area and void fraction of the skeleton. The model of the fluid flow is shown for the same skeleton permeability values as Figure 4, with the fluid properties of the liquid metal substituted for those of oil.

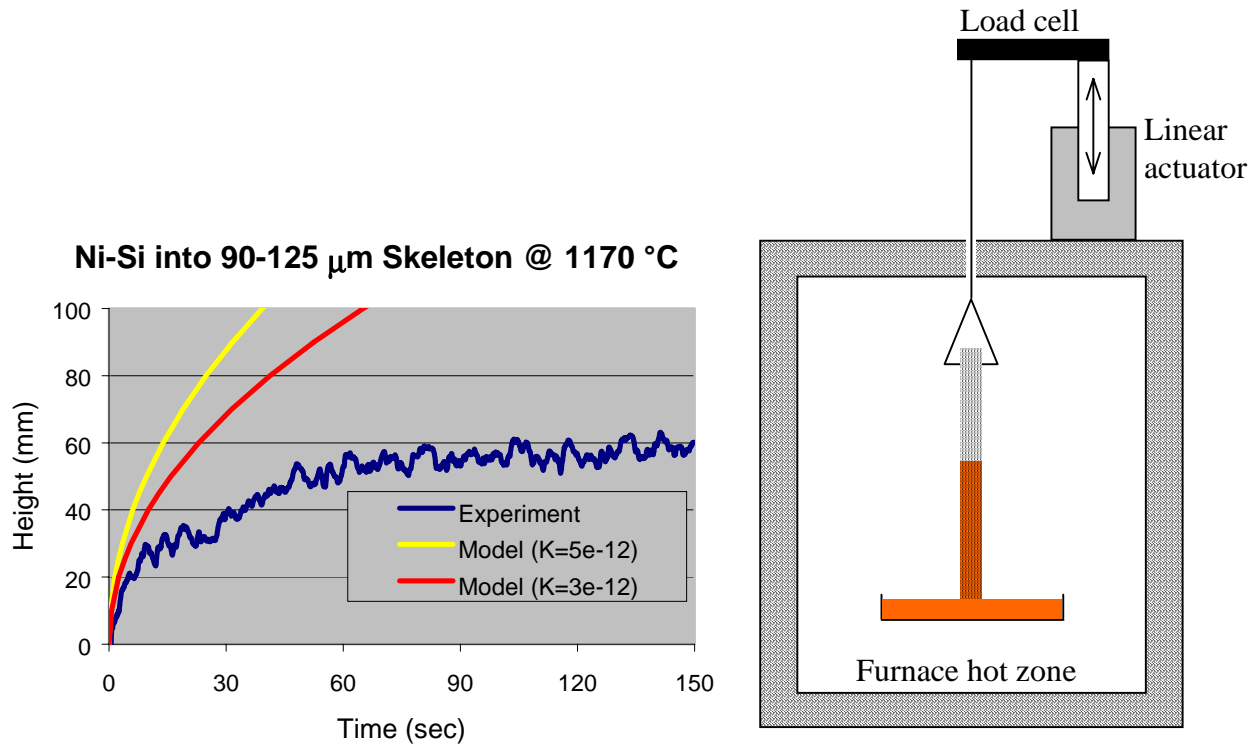


Figure 5: Infiltration rate experiments with molten metal and mass measurement setup.

Comparison of Figures 4 and 5 demonstrates that the time scale of the liquid metal infiltration is much faster than for infiltration with oil. This difference arises because the surface tension is ~50 times greater for the liquid metal. The significant deviation of the experimental results in Figure 5 from the model prediction can be explained by the “choking” effect of the infiltrant solidifying as it flows into the part. The next section will describe the attempt to characterize this solidification behavior.

### Solidification Quenching Experiments

The solidification rate was measured experimentally through a series of quenching experiments. A bundle of 50  $\mu\text{m}$  diameter nickel wires was sintered and then the bundle was dipped into a bath of molten Ni–10Si infiltrant. After holding at the infiltration temperature for variable time periods, the samples were air quenched. The samples were then sectioned and electropolished to reveal the microstructures shown in Figure 6 below. Wire was used instead of powder so that the motion of the solidification front could be referenced to the initial wire diameter and all motion would be perpendicular to the cross-sectioned view. Dashed white lines have been superimposed on the images to show the initial wire diameter. The outward progression of the solidification front can be seen by comparing the pictures in sequence. The

area with a eutectic microstructure reveals the part of the sample that was liquid at the time of the quench, and is bordered by the solidification front. The black crevice that appears within the dashed white circle is an effect of the electropolishing used to reveal the microstructure. The crevice corresponds to the distance to which silicon diffused into the initially pure nickel powder. A planar diffusion couple would result in a compositional profile of an error function with characteristic diffusion distance  $\sqrt{4D \cdot t}$ . For a diffusivity of silicon through nickel of  $7.85 \times 10^{-14} \text{ m}^2/\text{s}$  at  $1180^\circ\text{C}$ ,<sup>4</sup> this distance would be 1.8, 5.6 and 9.7 microns for 10, 100 and 300 seconds respectively. These expected diffusion distances correspond reasonably well with the observations in Figure 6, especially considering the difference in geometry.

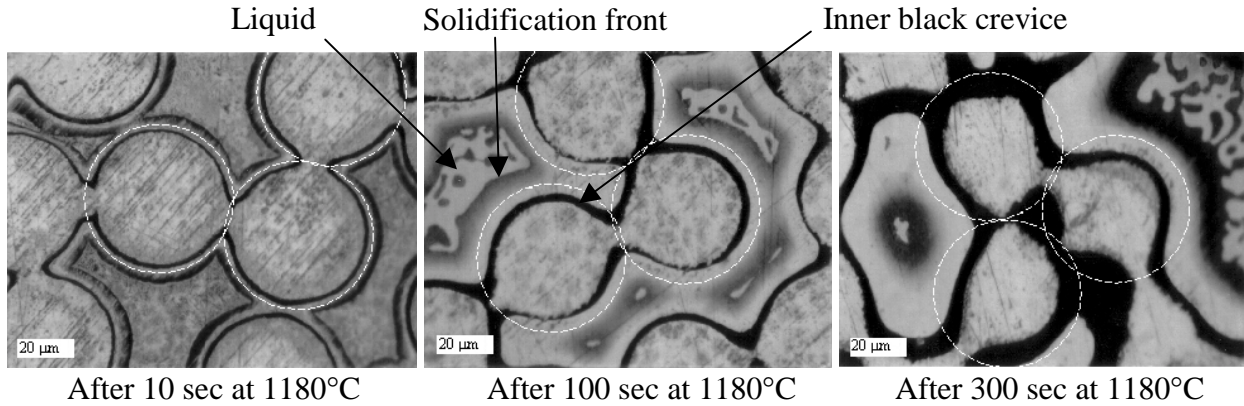


Figure 6: Optical micrographs showing sequence of infiltrated bundles of  $50 \mu\text{m}$  nickel wire.

### Infiltration Distance Limits

In order to maximize the distance the infiltrant can reach before freezing in TLI, a gating mechanism is used to prevent the infiltrant from contacting the skeleton prior to infiltration. Premature contact would allow diffusion to occur and the infiltrant to freeze just as it begins to melt. Other problems could arise if liquid begins to flow before the system has reached thermodynamic equilibrium. Several gating mechanisms have been used in practice such as dipping a suspended part into the melt or initial confinement of the melt followed by opening up a path for the melt to flow out and contact the skeleton.

The particle diameter of the powder affects both the fluid flow and the amount of time before the infiltrant freezes. Equation 3 describes the fluid flow behavior and because the permeability of a skeleton ( $K$ ) is proportional to the square of the powder diameter the net result of using larger powder is faster liquid flow. Further, the larger powder decreases the surface area for diffusion and provides more time for liquid to flow before the porous network is closed off by solidification. Figure 7 clearly shows how the infiltration distance (in this case height) is affected by the powder size of the skeleton. The capillary rise limit shown corresponds to the maximum height in Equation 1 with liquid metal properties of  $\gamma = 1.2 \text{ N/m}$  and  $\rho = 8 \text{ g/cc}$  and a void fraction of  $\varepsilon = 0.4$ . The rise limit will remain fairly consistent with different materials because many liquid metals have similar surface tension and density. The premature freezing limit shown corresponds to the experiments shown to the right using various powder sizes. Through the use of progressively larger powder size, infiltration heights as tall as 22 cm have been achieved. The freezing limit will vary significantly for different material systems because

it is affected by other properties such as the diffusivity of the melting point depressant in the skeleton, which can vary by several orders of magnitude.

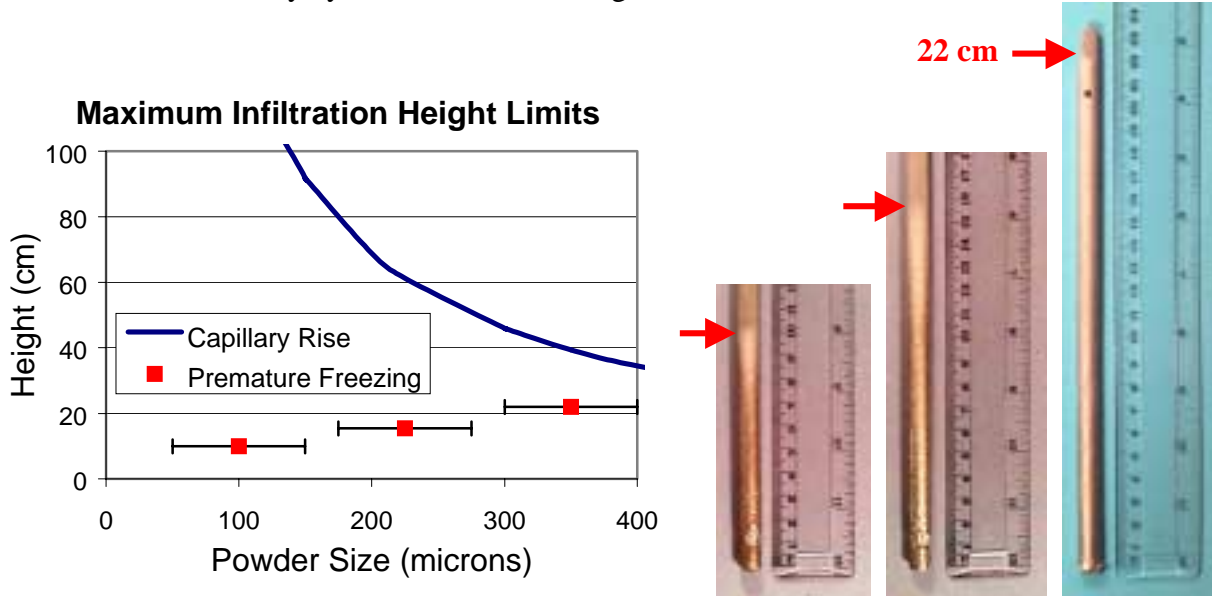


Figure 7: Limitations on infiltration height. Images at right show heights achieved with skeletons of 50–150µm, 150–300µm, and 300–400µm powder (left to right).

**Uniform bulk composition throughout the part**

Due to mass transport occurring simultaneously with the fluid transport within a part during transient liquid-phase infiltration, there exists the possibility of non-uniform bulk composition in a final part, with a higher concentration of silicon expected near the point of liquid entry. In order to prevent this variation, the liquid infiltrant can be maintained at a liquidus composition. This will ensure that any liquid present in the skeleton will be the same composition — any loss of silicon must result in solidification. Further, the liquid is already saturated with nickel and has no driving force for dissolution of the skeleton, preventing erosion.

Several techniques have been used to hold the composition of the infiltrant at its equilibrium liquidus composition and prevent it from dissolving the skeleton. Excess Ni powder was added to the melt in sufficient quantities that the bulk composition would be a mixture of saturated liquid and solid at the infiltration temperature. The supply of infiltrant was then soaked at a temperature slightly above the infiltration temperature to dissolve the excess nickel. A ceramic impeller was used to stir the melt and ensure the infiltrant supply was well mixed as the temperature was decreased again for the infiltration. The composition of parts infiltrated with infiltrant at its liquidus composition show no signs of erosion and have a bulk composition that does not change along the path of infiltration. This is further illustrated in Figure 8, showing a capillary infiltrated with infiltrant at its

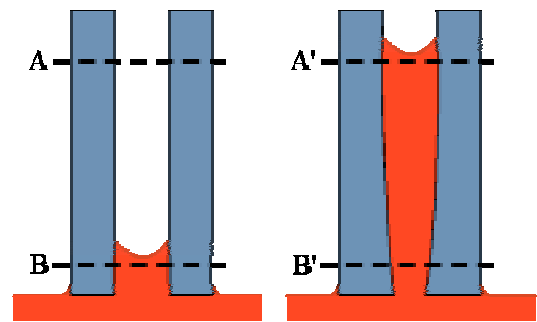
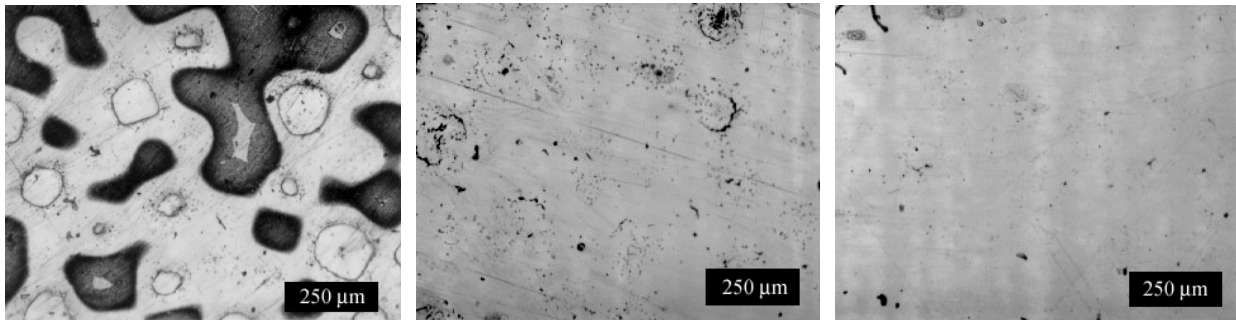


Figure 8: Uniform bulk composition along path of infiltration

liquidus composition. The composition profile at a point just behind the infiltration front (cross-section B) would consist of pure nickel and infiltrant at its liquidus composition because very little time has elapsed to allow for diffusion. After the liquid has continued to fill the capillary, a similar location just behind the infiltration front at cross-section A' would have an identical composition profile to B. Even though some diffusional solidification will occur at B' while the liquid is still infiltrating, the fixed composition of the liquid ensures that the bulk or average composition will be the same at point B, A', and B' — constant with time and position.

### **Homogenization and mechanical properties**

The time necessary for homogenization of a final part will depend strongly on the diffusivity of the melting point depressant and the geometry or powder size. Figure 9 shows cross-sections of a skeleton of ~300  $\mu\text{m}$  diameter powder that was infiltrated with Ni–10Si at 1170°C. The three sections of the infiltrated skeleton shown were heat treated at 1200°C for 1, 5 and 12 hours (left to right). Compositional analysis was conducted using an electron microprobe. The dark regions of the initial image correspond to high silicon content (>6%). After 5 hours of heat treatment, the compositional profile was nearly uniform, but regions of localized porosity are visible in the image — perhaps due to differential mass transport (Kirkendall effect). After 12 hours of heat treatment, the composition is uniform and any remaining porosity is evenly distributed.



*Figure 9: Homogenization of infiltrated 300 $\mu\text{m}$  powder after 1, 5, and 12 hours at 1200°C.*

The binary Ni–Si alloy used for these experiments is not available commercially and expectations for mechanical properties were not high. Comparison of an infiltrated specimen to a casting of identical composition showed that the transient liquid-phase infiltration process could produce a final material with similar properties. Tensile specimens were machined from an infiltrated bar homogenized for 12 hours and from a cast bar cooled at 5 °C/min from 1400°C. The tensile test results are shown in Figure 10 along with an image of the infiltrated specimen after failure. The elastic behavior and yield strength of both materials were nearly identical. The elongation of the infiltrated specimen was moderate at 6%, but still much less than that of the cast specimen. The mechanism causing the different behavior under high strain is not yet understood, but could be due to differences in porosity.

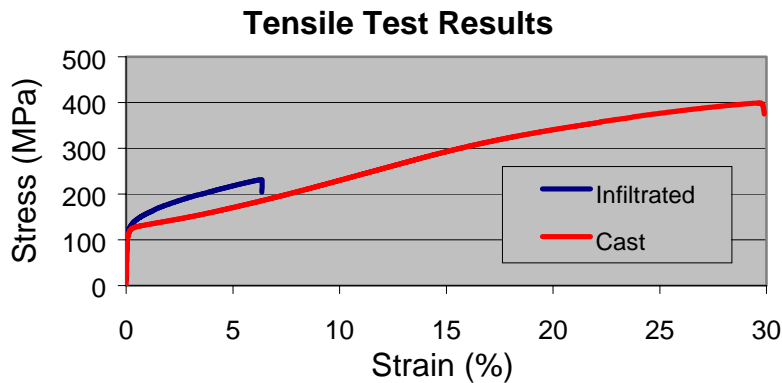


Figure 10: Tensile properties for infiltrated and cast specimens of the Ni – 4wt% Si. Image at right shows the infiltrated tensile specimen after failure.

### Summary

Transient liquid-phase infiltration of a PM skeleton has been shown to achieve homogeneous final part composition without the dimensional change associated with full-density sintering. This densification concept is broadly applicable to any of the SFF processes that produce green PM skeletons, as well as more traditional PM processes such as Metal Injection Molding. A binary Ni–Si alloy was used to explore the important tradeoff between infiltration and diffusion rate that can prevent the liquid from filling the part due to diffusional solidification. Using infiltrant at a liquidus composition ensures uniform bulk composition throughout the part. Through gated introduction of the liquid infiltrant to the skeleton and control of powder size within the skeleton, parts greater than 20 cm tall were infiltrated to full density. Subsequent heat treatment achieved a homogeneous final composition and the mechanical properties compared favorably to a cast specimen of the same composition.

### Acknowledgments

This research was sponsored by the Office of Naval Research, Contract #N00014-99-1-1090. The measurements of permeability and infiltration rate with oil were conducted by Vinay Prabhakar, a graduate student in the 3-D Printing research lab at MIT.

<sup>1</sup> Alloy Phase Diagrams. ASM Handbook Vol. 3. Metals Park, Ohio: American Society of Metals, 1992. pp 2-318

<sup>2</sup> Scherer, George W. “Theory of Drying” *J. Am. Ceram. Soc.*, Vol 73, No. 1, 1990. pp 3–14.

<sup>3</sup> Heinzer, Peter J. “Permeametry.” Powder Metallurgy. ASM Handbook Vol. 7. Metals Park, Ohio: American Society of Metals, 1984. pp 263-265.

<sup>4</sup> Smithells, Colin J. Smithells Metals Reference Book. 6<sup>th</sup> Edition. London, UK: Butterworths, 1983.